




## Article

# Synthesis, Structure and Impact of 5-Aminoorotic Acid and Its Complexes with Lanthanum(III) and Gallium(III) on the Activity of Xanthine Oxidase

Lozan Todorov <sup>1,\*</sup>, Luciano Saso <sup>2</sup>, Khedidja Benarous <sup>3</sup>, Maria Traykova <sup>4</sup>, Abderahmane Linani <sup>3</sup> and Irena Kostova <sup>1</sup>

<sup>1</sup> Department of Chemistry, Faculty of Pharmacy, Medical University, 1000 Sofia, Bulgaria; irenakostova@yahoo.com

<sup>2</sup> Department of Physiology and Pharmacology “Vittorio Ersparmer”, Faculty of Pharmacy and Medicine, Sapienza University, 00185 Rome, Italy; luciano.saso@uniroma1.it

<sup>3</sup> Laboratoire des Sciences Fondamentales, Université Amar Telidji, Laghouat 03000, Algeria; k.benarous@lagh-univ.dz (K.B.); abde.linani@lagh-univ.dz (A.L.)

<sup>4</sup> Department of Physics and Biophysics, Faculty of Medicine, Medical University, 1431 Sofia, Bulgaria; mlvtraykova@gmail.com

\* Correspondence: ltodorov@pharmfac.mu-sofia.bg

**Abstract:** The superoxide radical ion is involved in numerous physiological processes, associated with both health and pathology. Its participation in cancer onset and progression is well documented. Lanthanum(III) and gallium(III) are cations that are known to possess anticancer properties. Their coordination complexes are being investigated by the scientific community in the search for novel oncological disease remedies. Their complexes with 5-aminoorotic acid suppress superoxide, derived enzymatically from xanthine/xanthine oxidase (X/XO). It seems that they, to differing extents, impact the enzyme, or the substrate, or both. The present study closely examines their chemical structure by way of modern methods—IR, Raman, and <sup>1</sup>H NMR spectroscopy. Their superoxide-scavenging behavior in the presence of a non-enzymatic source (potassium superoxide) is compared to that in the presence of an enzymatic source (X/XO). Enzymatic activity of XO, defined in terms of the production of uric acid, seems to be impacted by both complexes and the pure ligand in a concentration-dependent manner. In order to better relate the compounds’ chemical characteristics to XO inhibition, they were docked in silico to XO. A molecular docking assay provided further proof that 5-aminoorotic acid and its complexes with lanthanum(III) and gallium(III) very probably suppress superoxide production via XO inhibition.

**Keywords:** lanthanum; gallium; coordination complex; superoxide; xanthine oxidase; enzyme inhibition; molecular docking



**Citation:** Todorov, L.; Saso, L.; Benarous, K.; Traykova, M.; Linani, A.; Kostova, I. Synthesis, Structure and Impact of 5-Aminoorotic Acid and Its Complexes with Lanthanum(III) and Gallium(III) on the Activity of Xanthine Oxidase. *Molecules* **2021**, *26*, 4503. <https://doi.org/10.3390/molecules26154503>

Academic Editor: Carlo Santini

Received: 30 June 2021

Accepted: 21 July 2021

Published: 26 July 2021

**Publisher’s Note:** MDPI stays neutral with regard to jurisdictional claims in published maps and institutional affiliations.



**Copyright:** © 2021 by the authors. Licensee MDPI, Basel, Switzerland. This article is an open access article distributed under the terms and conditions of the Creative Commons Attribution (CC BY) license (<https://creativecommons.org/licenses/by/4.0/>).

## 1. Introduction

The importance of the superoxide radical, O<sub>2</sub><sup>−</sup>, for human health and disease has been known for a long time [1–3]. It plays a crucial role in normal biological processes [4–8] as well as in the initiation of pathological conditions [9–16]. Extracellular superoxide radicals are characteristically released by cell types involved in immune defense, and also by many additional types of cells [17–19]. The formation of O<sub>2</sub><sup>−</sup> is inevitable in the living body. It is involved in a number of normal physiological processes as well as in cellular malignization, tumor proliferation, and malignant cell death [20,21].

The involvement of superoxide in cancer onset [22–25], development [26], and progression [27] is complex [28] and intensively explored [29]. Oxidative stress (OS)—the metabolic accumulation of free radicals dominating due to their deficient elimination—is typical for cancer cells [21,30]. OS is involved in carcinogenesis. It is also capable of helping eradicate malignant cells by varying their redox homeostasis.

Xanthine oxidase (XO) is one of the superoxide-producing enzymes. It is a homodimer with a molecular mass of 290 kDa. Belonging to the molybdenum protein family, it consists of two independent subunits, containing two separated substrate-binding sites [31]. Each subunit contains one flavin adenine dinucleotide (FAD), one molybdenum, and two iron–sulfur (2Fe-2S) centers of the ferredoxin type. XO catalyzes the oxidation of hypoxanthine to xanthine and subsequently to uric acid [32–34]. Throughout the reoxidation of XO, molecular oxygen acts as an electron acceptor, producing superoxide and hydrogen peroxide [35]. Control over superoxide formation and accumulation in the human body is essential for human health, therefore any effect on the activity of XO may impact the maintenance of healthy homeostasis.

Different approaches to control XO-generated superoxide have been explored in the search for efficient malignant cell elimination [36–38]. The goal of chemotherapy is to kill tumors by initiating apoptotic death [39–41]. That is achieved by raising oxidative stress levels in the tumor using a variety of drugs with pro-oxidant properties [42].

Lanthanide (Ln) ions induce cell membrane perforation and apoptosis, increase ROS-mediated oxidative damage, and alter the assembly and stability of the cytoskeleton. These effects make them potential pharmacological agents in cancer therapy [43]. Successful transport of lanthanide ions to the tumor has to be accompanied by some kind of mechanism to avoid their detrimental effect on healthy cells. These somewhat contradicting requirements characterize the search for new coordination compounds with improved antitumor activity and protective effects on normal cells [44,45]. One possible solution would be to use a coordination complex, comprising a highly pro-oxidant lanthanide cation, surrounded by bioactive ligands with antioxidant capacity. Such a complex has to be stable at a neutral, homeostatic pH and, at the same time, has to dissociate at acidic pH values that are typical for tumors. A number of complexes of gallium (Ga) and lanthanum (La) have been investigated in recent years for their pharmacological activities [46–50]. The Ga(III) and La(III) complexes with 5-aminoorotic acid have been shown to be stronger *in vitro* antioxidants, compared to the free ligand, at a normal, homeostatic pH [51–54].

In our previous investigations, we observed differing *in vitro* interactions of 5-aminoorotic acid and its complexes with superoxide, generated by different model systems [54,55]. Possible interactions of the compounds investigated with components of the superoxide-generating model systems were proposed. The aim of the present investigation is to look for a possible reason for the disparate superoxide-scavenging activity of 5-aminoorotic acid and its complexes with Ga(III) and La(III) in the presence of one non-enzymatic potassium superoxide (KO<sub>2</sub>) and one enzymatic xanthine/xanthine oxidase model systems. In both model systems, superoxide was the only free radical generated and its elimination was monitored using luminol-dependent chemiluminescence (LDCL). The radical-scavenging activity of a compound in the presence of the X/XO model system was compared with the activity of uric acid (UA) formation of the enzyme in the presence of the compound, estimated using UV spectroscopy.

A computer model of the interaction of 5-aminoorotic acid (HAOA) and its complexes with Ga(III)—GaAOA—and La(III)—LaAOA—with xanthine oxidase was developed using ChemDraw 16.0—a tool for generating chemical and biological drawings. It is the preferred tool for drawing chemical and biological concepts with metal atoms based on IUPAC, IUBMB, and CAS rules. It allows for calculating more than 100 chemical properties of a given structure. The complexes used in the work were prepared based on the Lewis and the Cahn–Ingold–Prelog (CIP) rules for stereochemistry structure and all the complexes were prepared and checked automatically by ChemDraw and saved in mol.2 format.

The complexes of lanthanum(III) and gallium(III) were synthesized by a reaction of Ga(III) and La(III) nitrates with 5-aminoorotic acid in amounts equal to a metal:ligand molar ratio of 1:3. The structures of the synthesized complexes were determined by means of spectral (FT-IR, FT-Raman, <sup>1</sup>H NMR) and elemental analysis. Since the crystal structure data are not available, theoretical approaches for determination of the geometrical parameters, vibrational frequencies, and the binding mode for the model M(III)–AOA

at a high level of theory are very helpful for extracting reliable structural information. Significant differences in the bands of the IR spectra of the complexes were observed and compared to the spectrum of the free ligand. A comparative analysis of the Raman spectra of the metal complexes with that of 5-aminoorotic acid allowed a good assignment of the vibrations of the functional groups involved in the coordination. The vibrational analysis, performed for the investigated species—5-aminoorotic acid and its metal complexes—helped explain the vibrational modes of the ligand, sensitive to interaction with the metals. The detailed vibrational study provided indication of the coordination behavior of the ligand to metal ions being in agreement with literature data and theoretical predictions.

## 2. Results

### 2.1. Chemistry

The compositions of the newly obtained metal complexes were characterized by elemental analysis. The nature of Ga(III) and La(III) complexes was confirmed by IR, Raman, and  $^1\text{H}$  NMR spectroscopy. The data from the elemental analysis of the obtained compounds served as a basis for the determination of their empirical formulas:  $\text{M}(\text{AOA})_3 \cdot 3\text{H}_2\text{O}$ , where  $\text{M} = \text{La}, \text{Ga}$  and  $\text{AOA}^- = \text{C}_5\text{N}_3\text{O}_4\text{H}_4^-$ .

The elemental analysis data of  $\text{La}(\text{AOA})_3 \cdot 3\text{H}_2\text{O}$  are shown as % calculated/found: C = 25.60/25.14; H = 2.56/2.24; N = 17.92/17.48;  $\text{H}_2\text{O} = 7.68/7.25$ ; La: 19.77/20.06, and for  $\text{Ga}(\text{AOA})_3 \cdot 3\text{H}_2\text{O}$ : C = 28.39/28.56; H = 1.89/2.02; N = 19.87/20.05;  $\text{H}_2\text{O} = 8.52/8.34$ ; Ga = 10.99/11.23, where  $\text{HAOA} = \text{C}_5\text{N}_3\text{O}_4\text{H}_5$  and  $\text{AOA} = \text{C}_5\text{N}_3\text{O}_4\text{H}_4^-$ .

#### 2.1.1. Vibrational Spectroscopy

The vibrational band assignments obtained from the IR and Raman spectra were analyzed by comparing them with those from the literature [56–79] and they were in agreement with the results of our DFT calculations (i.e., harmonic vibrational wavenumbers and Raman scattering activities) [80]. In Table 1, the selected calculated and experimental IR and Raman data in conjunction with their tentative assignment are given. The chemical structure of 5-aminoorotic acid is presented in Figure 1.

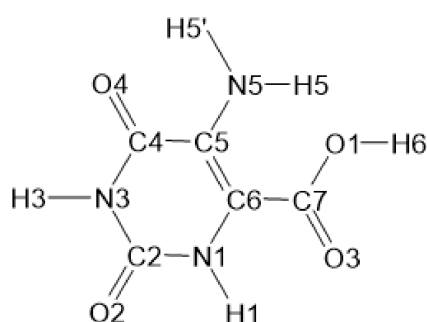


Figure 1. Chemical structure of 5-aminoorotic acid.

In the spectral region from  $3600\text{--}2000\text{ cm}^{-1}$  of the IR spectrum, the C-H and N-H stretches give rise to medium IR bands. In the IR spectra, the strong band at  $3457\text{ cm}^{-1}$  (for the 5-aminoorotic acid) and the medium bands for the La(III) and Ga(III) complexes were assigned to the N-H stretching modes of the pyrimidine rings (Table 1), while the band at  $3333\text{ cm}^{-1}$  (strong) in the IR spectrum of 5-aminoorotic acid, along with the band at  $3348\text{ cm}^{-1}$  (weak/medium) of the IR spectrum of the La(III) complex, and the band at  $3336\text{ cm}^{-1}$  (medium) of the IR spectrum of the Ga(III) complex, were attributed to the C-H stretching modes [56,74] (Table 1). In the Raman spectra of the ligand and metal complexes, the C-H and N-H vibrations were observed as follows: the N3-H3 stretching mode at  $3456\text{ cm}^{-1}$  and the C-H stretching mode at  $3323\text{ cm}^{-1}$  (Raman spectrum of the ligand); the N1-H1 stretching mode at  $3478\text{ cm}^{-1}$  (Raman spectrum of the La(III) complex) and the C-H stretching mode at  $3334\text{ cm}^{-1}$  (Raman spectrum of the Ga(III) complex). The

asymmetrical NH<sub>2</sub> stretch, absent in the IR spectrum of the ligand, can be seen in the vibrational spectra of the complexes at 3361 cm<sup>-1</sup> and 3355 cm<sup>-1</sup> as medium bands (IR spectra of La(III) and Ga(III) complexes) and at 3357 cm<sup>-1</sup> and 3358 cm<sup>-1</sup> as weak bands (Raman spectra of La(III) and Ga(III) complexes), whereas the symmetrical NH<sub>2</sub> stretch can be detected in the IR spectra of the ligand and metal complexes by signals with medium intensities, at 3196 cm<sup>-1</sup> (ligand), 3171 cm<sup>-1</sup> (La(III) complex), 3168 cm<sup>-1</sup> (Ga(III) complex) and only in the Raman spectrum of the ligand as a very weak band at 3166 cm<sup>-1</sup> [60]. The 2700–3000 cm<sup>-1</sup> wavenumber region of the IR spectra of 5-aminoorotic acid and its complexes is characteristic of strongly hydrogen-bonded intermolecular complexes [60–62].

**Table 1.** Selected experimental IR and Raman wavenumbers (cm<sup>-1</sup>) of 5-aminoorotic acid (HAOA) and its La(III) and Ga(III) complexes [LaAOA, GaAOA] and their tentative assignment. Abbreviations: vw—very weak; w—weak; m—medium; ms—medium strong; s—strong; vs—very strong; sh—shoulder;  $\nu$ —stretching;  $\delta$ —bending;  $\tau$ —torsion; s—symmetric; as—asymmetric; def.—deformation; ip—in plane; op—out of plane; ring—pyrimidine ring; sciss—scissoring; wagg—wagging; M—metal.

IR			Raman			Vibrational Assignment
HAOA	LaAOA	GaAOA	HAOA	LaAOA	GaAOA	
3457 s	3479 w	3443 w	3479 w	3478 vw		$\nu$ (N1H1)
	3361 m	3355 m	3456 vw	3357 w	3358 w	$\nu_{as}$ (NH <sub>2</sub> )
3333 s	3448 w	3336 m	3323 m		3334 w	$\nu$ (N3H3), $\nu$ (C-H)
3196 m	3171 m	3168 m	3166 vw			$\nu_s$ (NH <sub>2</sub> )
1691 vs	1718 m	1717 m	1698 m			$\delta$ (NH); $\nu_s$ (C2=O2), $\nu$ (N-C6)
	1684 vs	1691 vs				$\nu_s$ (C4=O4)
1667 s	1673 vs	1676 vs	1678 sh	1673 m	1682 m	$\nu_s$ (C4=O4); $\nu$ (COO <sup>-</sup> ), $\nu$ (C5=C6), $\delta$ (N3-H3)
1604 s	1637 vs	1645 vs	1612 vs	1623 vs	1628 vs	$\nu$ (C5=C6); $\beta$ (NH <sub>2</sub> ), $\nu$ (COO <sup>-</sup> )
1566 m	1556 m	1553 m	1560 m	1542 w/m	1546 w/m	$\delta_{ip}$ (N1H1, N5H5); $\nu$ (C5C6), $\beta_s$ (NH <sub>2</sub> )
1511 w	1499 m	1498 m	1492 w/m	1494 w	1501 w	$\delta$ (NC); $\nu$ (ring); $\delta_{ip}$ (N3H3)
1457 m			1447 w		1433 w	$\nu$ (ring), $\beta_s$ (NH <sub>2</sub> ), $\delta$ (N1-H1), $\nu$ (COO <sup>-</sup> )
1436 m	1424 s	1425 s	1421 w	1420 vs	1407 vs	$\delta$ (N3H3), $\delta$ (ring), $\delta$ (N1H1)
1405 m	1390 s	1391 s		1384 s	1388 s	$\delta$ (N3H3), $\delta$ (ring), $\delta$ (N1H1), $\nu_s$ (COO <sup>-</sup> )
1312 m	1306 m	1306 m	1301 w	1295 m/s	1302 m/s	$\nu$ (C5-N), $\nu$ (C-N), $\delta$ (OH), $\beta_s$ (NH <sub>2</sub> )
1255 m/s	1290 sh	1284 sh				$\nu$ (C-N), $\delta$ (N1H1), $r$ (NH <sub>2</sub> ), $\delta$ (ring)
1234 m/s	1237 w	1239 w	1242 m	1230 m/s	1240 m/s	$\nu$ (C-N), $\delta$ (N3H3), $r$ (NH <sub>2</sub> ), $\delta$ (N1H1)
1140 sh	1122 vw	1126 vw		1124 vw	1131 vw	$\delta$ (OH)
1083 vw			1047 vw	1041 w	1044 w	$\nu$ (C6-O, C6-C7), $\beta_{as}$ (NH <sub>2</sub> )
989 sh						$\nu$ (NCN), $\delta$ (N3H3), $r$ (NH <sub>2</sub> ), $\delta$ (N1H1)
924 w	941 sh	944 sh	919 w/m	933 w/m	948 w/m	$\nu$ (NCC), $\nu$ (ring), $r$ (NH <sub>2</sub> ), $\nu$ (COO)
871 w/m	884 vw	875 vw				$\gamma$ (N3-H3), $\gamma$ (ring)
795 vw	798 m/807	797 m/807	809 vw	788 sh	781 sh	$\delta_{op}$ (O3C7O1)
767 vw	775 w	777 w		763 m	777 m	$\gamma$ (C4=O4), $\gamma$ (C4-C=C6), $\gamma$ (C6-C12)
754 w	759 w	759 w	749 vw			$\gamma$ (C6-C12), $\gamma$ (C4=O4), $\gamma$ (COOH), $\gamma$ (N3-H)
740 w	747 w	749 w				$\gamma$ (C2=O2), $\gamma$ (NC2N), $\gamma$ (N3-H)
696 vw	694 vw	692 vw				$\delta$ (ring), $\Delta_s$ (COO), $r$ (NH <sub>2</sub> )
	617 vw	602 vw				$\nu$ (M-O)
584 vw		595 vw	582 w	581 w/m	589 w/m	$\delta$ (ring), $\Delta_s$ (COO)
	521 sh	509 sh				$\nu$ (M-O)
488 w		501 w	482 w/m	480 m	495 m	$\delta$ (ring), $\delta$ (NH <sub>2</sub> ), $\Delta_s$ (COO)
474 w/m	459 sh	465 sh				$\gamma$ (OH)
446 m	441 m	442 m	445 w			$\delta$ (OCNCO), $\delta$ (COO) + $r$ (NH <sub>2</sub> )
	422 sh	422 sh	425 sh	425 w/m	438 w/m	$\tau$ (C2O2, ring), $\Delta_{as}$ (COO)
						$\delta$ (OCCN11), $\delta$ (COO), $\delta$ (C2=O),
			381 vw	375 w	374 w	$r$ (NH <sub>2</sub> ); $\nu$ (M-O)
						$\nu$ (M-O)
			249 w	339 sh	243 w	$\tau$ (NH <sub>2</sub> ), $\Delta_s$ (COO)
				224 w	205 w	$\nu$ (O-M-O)
			196 w	192 sh	182 sh	$\tau$ (ring); $\delta$ (O-M-O)



A very strong band at  $1691\text{ cm}^{-1}$  in the IR spectrum of 5-aminoorotic acid and two strong bands at  $1718\text{ cm}^{-1}$  and  $1684\text{ cm}^{-1}$  in the IR spectrum of the La(III) complex and at  $1717\text{ cm}^{-1}$  and  $1691\text{ cm}^{-1}$  in the IR spectrum of the Ga(III) complex could be detected in the  $1730\text{--}1690\text{ cm}^{-1}$  region, which were assigned to the symmetrical C2=O2 and to the N-H stretching modes. Opposite to the IR spectra, in the same region of the Raman spectra, only one medium band at  $1698\text{ cm}^{-1}$  for the ligand was observed.

The detected strong band at  $1667\text{ cm}^{-1}$  (IR spectrum of 5-aminoorotic acid) and the two very strong bands for each of the complexes, at  $1673\text{ cm}^{-1}$  and  $1637\text{ cm}^{-1}$  (IR spectrum of La(III) complex) and at  $1676\text{ cm}^{-1}$  and  $1645\text{ cm}^{-1}$  (IR spectrum of Ga(III) complex), were assigned to the symmetrical stretching C4=O4 modes [62] and to the asymmetrical COO<sup>-</sup> stretching modes [60,68]. In the respective Raman spectra, these vibrations can be found as a shoulder at  $1678\text{ cm}^{-1}$  for the ligand, as a medium band at  $1673\text{ cm}^{-1}$  for its La(III) complex, and as a medium band at  $1682\text{ cm}^{-1}$  for its Ga(III) complex (Table 1). In the IR spectrum of 5-aminoorotic acid, the strong band at  $1604\text{ cm}^{-1}$  was attributed to the C5-C6 stretching contributions and NH<sub>2</sub> scissoring [60,62], whereas in the IR spectra of the metal complexes are absent. In the Raman spectra, these vibrations are presented as very strong bands at  $1612\text{ cm}^{-1}$  for 5-aminoorotic acid and at  $1623\text{ cm}^{-1}$  for its La(III) complexes and  $1628\text{ cm}^{-1}$  for its Ga(III) complexes (Table 1).

The IR bands with medium relative intensities at  $1566\text{ cm}^{-1}$  (ligand),  $1556\text{ cm}^{-1}$ , and  $1553\text{ cm}^{-1}$  (La(III) and Ga(III) complexes), as well as the medium bands in the Raman spectra, at  $1560\text{ cm}^{-1}$  (ligand),  $1542\text{ cm}^{-1}$ , and  $1546\text{ cm}^{-1}$  (La(III) and Ga(III) complexes), were assigned to the C5-C6 stretching and in plane N-H bending modes (Table 1). The pyrimidine ring vibrations (N-C and N-H bending modes) were found as follows: a weak peak at  $1511\text{ cm}^{-1}$  (IR spectrum of 5-aminoorotic acid), a medium band at  $1499\text{ cm}^{-1}$  (IR spectrum of the La(III) complex), and a medium signal at  $1498\text{ cm}^{-1}$  (IR spectrum of the Ga(III) complex), while in the Raman spectra these vibrational modes were detected for the ligand as a weak/medium band at  $1492\text{ cm}^{-1}$  and as weak signals at  $1494\text{ cm}^{-1}$  and  $1501\text{ cm}^{-1}$  for its La(III) and Ga(III) complexes, respectively (Table 1). Other in-plane N-H bending modes were observed only in the IR and Raman spectra of the ligand or in both spectra types (Table 1). The symmetrical COO<sup>-</sup> stretching mode was detected in the IR spectra as a medium signal at  $1405\text{ cm}^{-1}$  for 5-aminoorotic acid and as strong bands at  $1390\text{ cm}^{-1}$  and  $1391\text{ cm}^{-1}$  for its La(III) and Ga(III) complexes, while in the Raman spectra this vibrational mode appears only for the metal complexes as strong signals at  $1384\text{ cm}^{-1}$  and  $1388\text{ cm}^{-1}$  (La(III) and Ga(III) complexes, Table 1).

The very weak band at  $989\text{ cm}^{-1}$  in the ligand IR spectrum (absent in the IR spectra of the complexes), which corresponds to the trigonal pyrimidine ring breathing mode [56,60], cannot be observed in the respective Raman spectra of the studied compounds. The weak band in the ligand IR spectrum ( $924\text{ cm}^{-1}$ ) and the very weak bands at  $941$  and  $944\text{ cm}^{-1}$  in the IR spectra of the metal complexes, as well as the weak/medium band at  $919\text{ cm}^{-1}$  (Raman spectrum of the ligand) and the weak bands at  $933$  and  $948\text{ cm}^{-1}$  in the metal complex Raman spectra, were assigned to the out of plane C-C and C-N bending modes.

As a whole, from the comparison between the vibrational spectra of the ligand and the comparable spectra of the metal complexes, we can emphasize wavenumber shifting, with increases and/or decreases in their relative intensities, as well as appearances and/or disappearances of several bands. The observed changes can be caused by the decrease in the force constants of the C-C and C-H bonds and their polarization in the pyrimidine rings [71]. The complex formation with metals perturbs the ring aromatic and quasi-aromatic systems [81]. The metal affects the metal–oxygen bonds, and this effect is relocated to the C-O bonds. Subsequently, the force constant of the OCC<sub>ring</sub> bond is changed, which reproduces the displacement of the electronic charge around bonds between heterocyclic rings, and heterocyclic rings and protons [82].

The ligand's pyrimidine ring bending vibrations and the skeletal deformation bands in the  $900\text{--}300\text{ cm}^{-1}$  wavenumber region show significant changes in coordination (Table 1). These changes may be connected with the distortion of the pyrimidine rings upon complex

formation. Additionally, the spectra in the frequency region under  $600\text{ cm}^{-1}$  are quite interesting, since they offer information about metal–ligand vibrations. The new detected bands in the complexes' IR spectra, at  $617\text{ cm}^{-1}$  (La(III) complex) and at  $602\text{ cm}^{-1}$  (Ga(III) complex), as well as the new shoulders at  $521\text{ cm}^{-1}$  (La(III) complex) and  $509\text{ cm}^{-1}$  (Ga(III) complex), which are not observable in the Raman spectra, can be attributable to the M–O interactions [60,62,79]. The metal disturbs the carboxylate anion as well as the whole ring structure. The metal ionic potential is the most significant parameter, responsible for the metal influence on the rest of the organic molecule [82–84]. It is known that carboxylic acids interact with the metals as symmetric [85,86], bidentate carboxylate anions and both oxygen atoms of the carboxylate are symmetrically bonded to the metal [87]. In this sense, we could detect, in the low-wavenumber region of the Raman spectra of the La(III) and Ga(III) complexes, weak bands at  $224, 192\text{ cm}^{-1}$  and  $205, 182\text{ cm}^{-1}$ , respectively, which can be attributed to the O1–M–O3 vibration modes (Table 1) [88–90].

### 2.1.2. $^1\text{H}$ NMR Spectra of the Ligand and Its Metal Complexes

The coordination of the metal ions with the ligand's carboxylate oxygen atoms was demonstrated with the help of the data of  $^1\text{H}$  NMR spectra. Proton spectra recorded at 250 MHz in  $\text{DMSO-}d_6$  confirmed complex formation. The typical chemical shifts of the  $^1\text{H}$  NMR spectra in  $\text{DMSO-}d_6$  are presented in Table 2.

**Table 2.**  $^1\text{H}$  NMR (250 MHz,  $\text{DMSO-}d_6$ ).

$\text{N}_n\text{-H}$	HAOA	LaAOA	GaAOA
$\text{N}_1\text{-H}$	11.47	11.22	11.46
$\text{N}_3\text{-H}$	9.44	9.03	8.48
$\text{C}_5\text{NH}_2\text{-2H}$	6.00	5.57	5.33

The  $^1\text{H}$  NMR spectrum of 5-aminoorotic acid in  $\text{DMSO-}d_6$  demonstrates the expected three resonances which correspond to the NH protons. The carboxamido and imido protons have singlets at  $\delta_{\text{H}}$  11.47 and 9.44 and the amino protons provide a broad signal at  $\delta_{\text{H}}$  6.00 [72]. The amido and imido protons were also observed in the spectra of the complexes in the same solvent. The complexes' spectra show a very broad peak at ca.  $\delta_{\text{H}}$  3.4, which can be attributed to the intermolecular exchange of protons between the amino group and water (contained in the solvent). We did not observe two sharp signals of the separated species or an averaged signal which could be due to the intermediate rate of the exchange [91,92]. The observed  $\text{N}_3\text{-H}$  proton resonance in the NMR spectra (Table 2) clearly shows that this nitrogen atom is not involved in complex formation. Therefore, we can conclude that M(III) ions appear to bind the 5-aminoorotic acid at the carboxyl ion, as reported for most of the studied orotato complexes [68,71,91,92].

It can be concluded that, as has been reported previously for analogous complexes [72], the  $^1\text{H}$  NMR spectra of the new La(III) and Ga(III) complexes in  $\text{DMSO-}d_6$  showed the presence of one carboxamido, one imido, and two amino protons. Additionally, the complexes' signals in  $\text{DMSO-}d_6$  are quite similar in the regions of the NH and  $\text{NH}_2$  proton resonances. Proton NMR spectra of 5-aminoorotic acid and its La(III) and Ga(III) complexes confirmed the anticipated coordination of 5-aminoorotic acid via its carboxylate oxygen atoms [69,79].

### 2.2. Radical-Scavenging Assays

In order to elaborate on the possible reasons for the differing results when comparing scavenging of “non-enzymatic” superoxide  $\text{KO}_2$  to that of “enzymatic” X/XO, a brief review of previously published results [54,55] is provided. The radical-scavenging activity of a compound is illustrated by the CL-SI calculated after the LDCL experiments. It demonstrates the impact of the compounds on luminol-dependent luminescence. The lower the CL-SI, the higher the radical-scavenging activity. The activity in the UA formation

was monitored by the relative change in the absorption at 293 nm for a fixed period of time and is presented as a percentage of the same in the absence of the investigated compound. The lower the percentage, the lower the activity of UA formation.

The radical-scavenging activities of HAOA toward superoxide and the effect on the activity of XO to produce uric acid are summarized in Figure 2. All parameters measured were concentration dependent. In the presence of superoxide formed in the  $\text{KO}_2$  model system, HAOA was a pronounced scavenger. Noticeable scavenging activity was observed at concentrations above  $1 \times 10^{-6}$  M.

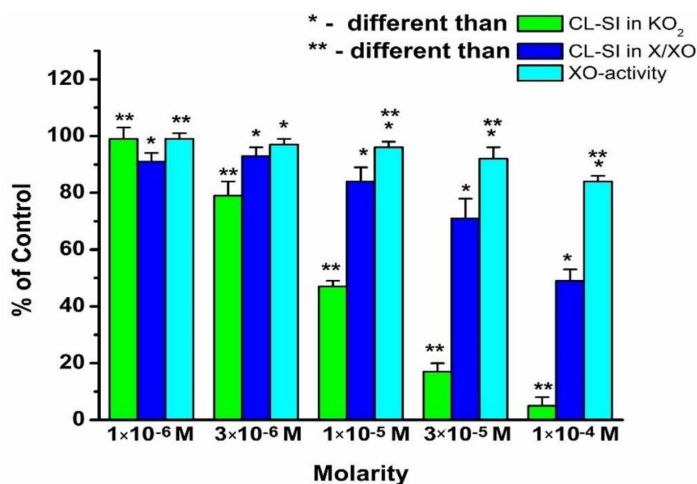


**Figure 2.** Radical-scavenging activity of HAOA toward superoxide radical formed in  $\text{KO}_2$  and X/XO model systems, and activity of XO in the formation of uric acid (UA) in the X/XO model system. Data = mean  $\pm$  StDev,  $p < 0.05$ .

In general, the scavenging activity of HAOA toward X/XO-generated superoxide was weaker than that toward  $\text{KO}_2$  generated superoxide. The enzymatic activity of XO (in terms of UA formation) in the model system X/XO was concentration dependent in a similar way to the scavenging activity. A noticeable difference between  $\text{O}_2^-$ -scavenging activity and activity of UA formation was observed at concentrations of HAOA of  $1 \times 10^{-5}$  M and above.

The radical-scavenging activity of GaAOA in the presence of the  $\text{KO}_2$  and X/XO model systems as well as the activity of XO in the UA formation are presented in Figure 3. Similar to Figure 2, all parameters observed were concentration dependent. In the presence of the  $\text{KO}_2$  model system, GaAOA behaves as a strong scavenger of superoxide radicals.

Within the entire interval of GaAOA concentrations, the radical-scavenging activity toward  $\text{KO}_2$ -generated superoxide was markedly higher than that toward the X/XO-generated radical. The activity of XO to produce UA in the presence of GaAOA was lower than that in the absence of the compound even at GaAOA concentrations as low as  $1 \times 10^{-6}$  M. A statistically significant difference between superoxide-scavenging activity and activity of UA formation in the presence of the X/XO model system was observed for GaAOA solutions of concentrations of  $1 \times 10^{-5}$  M and above. Figures 2 and 3 demonstrate that in the presence of the X/XO model system, the superoxide-scavenging activity of GaAOA was higher, while UA formation was lower than the same parameters in the presence of HAOA at the same concentration.

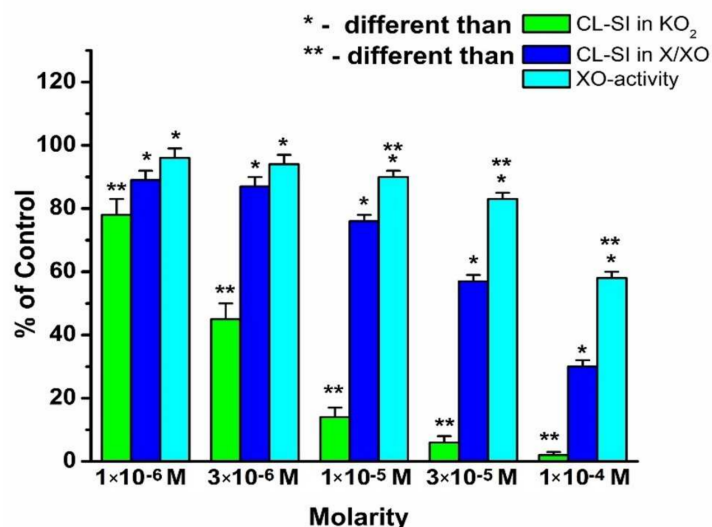


**Figure 3.** Radical-scavenging activity of GaAOA toward superoxide radicals formed in  $KO_2$  and X/XO model systems, and activity of XO in the formation of uric acid (UA) in the X/XO model system. Data = mean  $\pm$  StDev,  $p < 0.05$ .

The superoxide-scavenging activity and activity of UA formation in the presence of LaAOA are displayed in Figure 4.

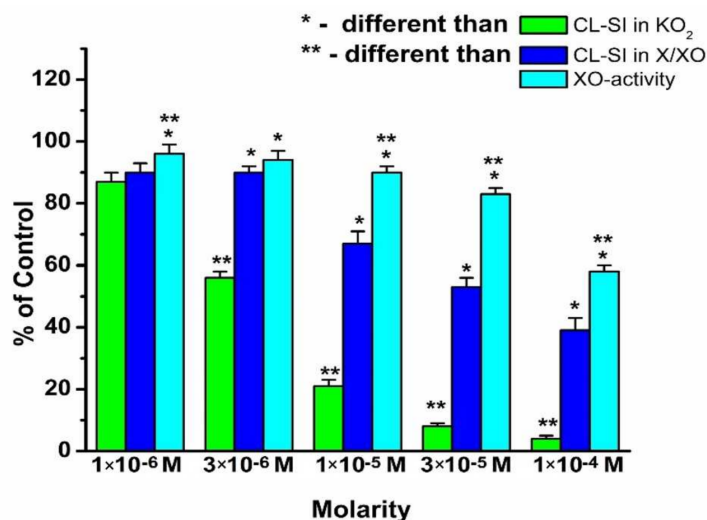


**Figure 4.** Radical-scavenging activity of LaAOA toward superoxide radicals formed in  $KO_2$  and X/XO model systems, and activity of XO in the formation of uric acid (UA) in the X/XO model system. Data = mean  $\pm$  StDev,  $p < 0.05$ .

All parameters monitored were concentration dependent. Within the entire concentration interval, LaAOA behaves as a scavenger of  $KO_2$ -generated superoxide. At a concentration of  $1 \times 10^{-6}$  M, the CL-SI was about 85–90%. In the presence of the X/XO model system, CL-SI decreased with the increase in the concentration of the complex. Above a concentration of  $1 \times 10^{-6}$  M, the  $O_2^-$ -scavenging activity of LaAOA in the X/XO model system was much lower than that in the  $KO_2$  model system. The activity of UA formation in the X/XO model system decreased with the increase in LaAOA concentrations. In the presence of  $1 \times 10^{-5}$  M LaAOA and higher, the activity of UA formation was markedly higher than the CL-SI for X/XO-generated superoxide. Figures 2 and 4 demonstrate that in the presence of the X/XO model system, the radical-scavenging activity

toward superoxide was higher, but the activity of the UA formation was lower than the corresponding parameters for same concentration of HAOA.

### 2.3. Molecular Docking Assay

We docked HAOA, GaAOA, and LaAOA into human xanthine oxidase (HXO) with PDB ID: 2CKJ. The docking center was set on Glu1262, Arg913, Gln768, and Arg881 according to Enroth et al. [93–95].

The results showed multiple solutions with up to 100 poses saved per molecule. The best GOLD PLPChem score was selected. The saved PLPChem scores were 34.42, 33.35, and 16.45 for lanthanum(III), gallium(III) complexes, and HAOA, respectively. The docking results showed that the lanthanum(III) complex interacted via a total of 14 hydrogen interactions, as well as five carbon–hydrogen interactions that were saved with the pyrimidine function, thus proving the importance of this function in maintaining stability inside the active site. Only five hydrophobic interactions were found with Ala and Cys amino acids. Gln768 saved an important distance of 1.30 Å, creating the possibility to form metal coordinations between the inhibitor and the enzyme since the ionic oxygen atoms were responsible for causing interactions with the most catalytic amino acids, thus promoting possible irreversible inhibition (Figure 5).

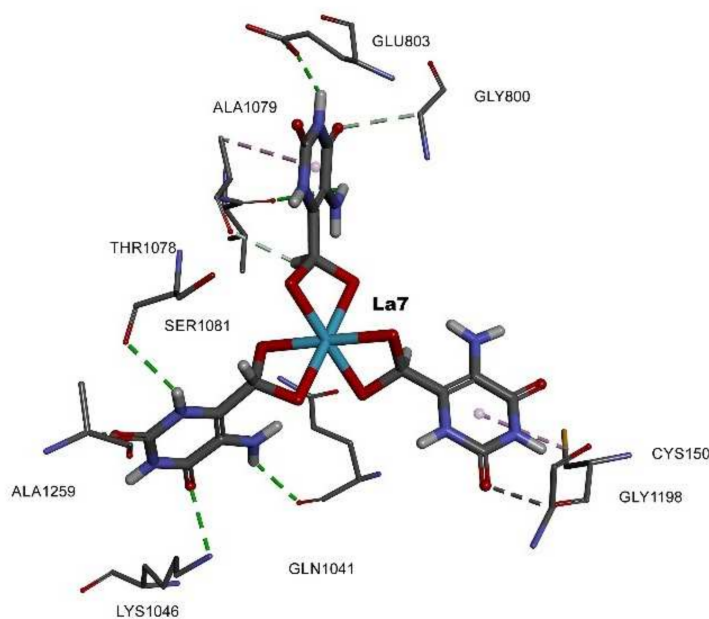


**Figure 5.** The 3D structure of the lanthanum (III) complex presented as sticks and colored by CPK with the involved amino acids inside the active site of the HXO.

The gallium(III) complex interacted with eight hydrogen interactions, Gln1041 saved one interaction, pi-donor hydrogen bond type, with the pyrimidine function and three hydrophobic interactions with Ala, Cys, and Phe. The mechanism of action of the gallium(III) complex saved was the same as for the lanthanum(III) complex since the only difference was the ion type, however, the chosen conformation to bind in the active site was slightly different with a repeated ratio (RR) of 90% (Table 1), which could affect the overall inhibition process (Figure 6).



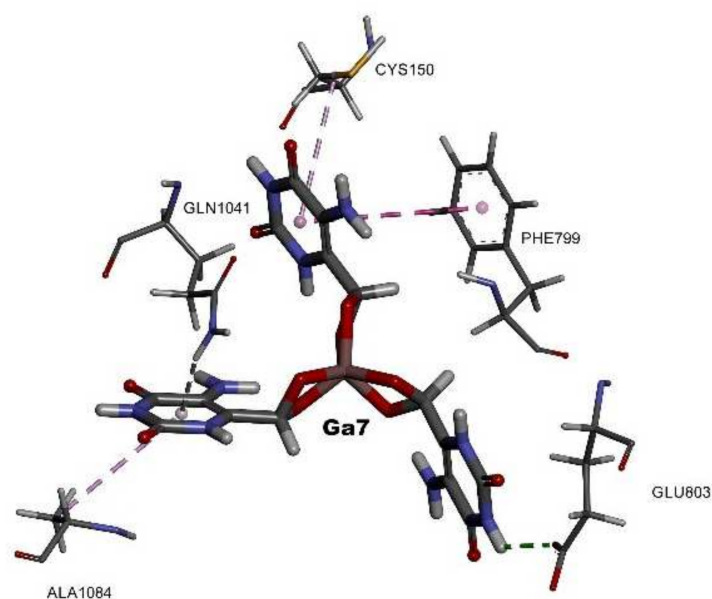


**Figure 6.** The 3D structure of the gallium(III) complex presented as sticks and colored by CPK with the involved amino acids inside the active site of the HXO.

HAOA (Table 3) forms one hydrogen interaction, the conventional hydrogen bond type, saved by Arg913 and one pi–sulfur interaction saved by Met1039 with the uracil group. The major difference between the two complexes (La and Ga) and HAOA was the number of uracil groups (three in the complexes), which can favor more interactions with the active site amino acids.

**Table 3.** The molecular docking results analysis.

Rank	Inhibitors	RR (%)	PLPChem Score	Nucleophilic Residues	Interaction Type	Length (Å)	Number of Interactions	Fav/Unfav Bond
Control	Allopurinol	100	23.89	GLY798	Hydrogen Bond	2.15	04	8/0
					Hydrophobic Bond	4.07	04	
1	LaAOA	100	34.42	GLN768	Hydrogen Bond	1.30	14	20/4
					Hydrophobic Bond	4.24	05	
					Coulombic	3.47	01	
2	GaAOA	90	33.35	GLN1195	Hydrogen Bond	1.90	12	15/01
					Hydrophobic Bond	4.46	03	
					Coulombic	/	00	
3	HAOA	100	16.45	ARG913	Hydrogen Bond	3.15	01	3/0
					Hydrophobic Bond	4.38	02	
					Coulombic	/	00	

PLPChem: piecewise linear potential; Fav/Unfav: favorable/unfavorable; RR: repetition ratio.

We docked allopurinol in the HXO in our previous work [96,97] as the reference inhibitor to compare it with the complexes under investigation.

### 3. Discussion and Conclusions

In summary, Figures 2–4 show that all three compounds behave as scavengers of superoxide radicals, generated in the presence of the  $KO_2$  and X/XO model systems in a concentration-dependent manner. The relative differences between the superoxide-scavenging activities of these compounds were in agreement with their previously observed affinity to participate in interactions with stable free radicals via electron transfer reactions [54,55].

The scavenging activity toward X/XO-generated superoxide of each compound at the same concentration is lower than that toward the  $KO_2$ -generated superoxide. It was proposed that this observation might be related to some kind of impact of the compounds

on the activity of the enzyme to produce uric acid, as the  $O_2^-$  radical is a by-product of UA formation. To explore this probability, a model system was created by using a molecular docking protocol that allows the molecules of HAOA, GaAOA, and LaAOA to interact with the molecule of xanthine oxidase. The reasoning behind this approach lies in the fact that the structure of 5-aminoorotic acid includes a pyrimidine ring that, theoretically, would allow the compound to adsorb onto the enzyme.

The standard inhibitor (allopurinol) exhibited interactions with the catalytic amino acids inside the active site via three hydrogen bonds, whereas the studied inhibitors have one to fourteen hydrogen bonds. The best inhibitor was chosen based on the highest PLPChem score, firstly, and secondly by the ratio of the most repeated poses (RR) as a percentage compared to the control (allopurinol), so, based on these results, LaAOA was the best inhibitor model for XO and GaAOA was moderate, while HAOA was the weakest inhibitor. Based on the present study, the following conclusions can be drawn:

1. HAOA, LaAOA, and GaAOA are all scavengers of superoxide, derived from  $KO_2$  and X/XO;
2. All three substances manifest higher superoxide-diminishing activity in the non-enzymatic model, compared to the enzymatic model;
3. All three substances diminish the production of UA in the X/XO model. Previously, we proposed that this may be due to an interaction between the substances and one/both elements of the model system;
4. Molecular docking suggested that all three substances interact with the active sites of XO, showing potential as enzyme inhibitors. The calculated strength of the interaction decreases in the order LaAOA > GaAOA > HAOA. This result corresponds well with the data from the XO activity UV assay—HAOA decreases UA formation by 15–20%, while both complexes cause a decrease of about 40–45%.
5. In the enzymatic models, superoxide diminishment is greater than the suppression of UA production. Since, for one molecule UA produced, one superoxide ion is generated, we can propose with a reasonable amount of certainty that in the X/XO model, HAOA, GaAOA, and LaAOA act as both:
  - superoxide scavengers, which is clear enough from the results, derived from the  $KO_2$  assay;
  - XO inhibitors, a proposition supported by the decrease in UA production in the X/XO model and also by the molecular docking assay. Another possible confirmation of that hypothesis comes from the fact that as molecular docking identified HAOA as the substance with weakest interaction with XO, that same substance caused the least diminishing of UA production in the enzymatic model.

## 4. Materials and Methods

### 4.1. Synthesis of the Complexes

The compounds used for the synthesis of the complexes were Merck products, p.a. grade:  $La(NO_3)_3 \cdot 6H_2O$  and  $Ga(NO_3)_3 \cdot 6H_2O$ . 5-Aminoorotic acid (Figure 1) was used as a ligand. The complexes were obtained via a reaction of lanthanum(III) and gallium(III) inorganic salts and the ligand, in amounts equal to a metal:ligand molar ratio of 1:3. The synthesis was carried out by adding aqueous solutions of La(III) and Ga(III) nitrates to the aqueous solution of the ligand, subsequently raising the pH of the mixture gradually to ca. 5.0 by adding dilute solution of NaOH. The formation of the metal complexes can be represented as the following chemical equations (1), (2):



where  $M = La, Ga$ ;  $HAOA = C_5N_3O_4H_5$ ; and  $AOA^- = C_5N_3O_4H_4^-$ .

The reaction mixture was stirred with an electromagnetic stirrer at room temperature for one hour. As a result of mixing of the solutions, the precipitates of the obtained

complexes were derived. They were filtered (pH 5.0), washed with water, and dried in a desiccator to a constant weight. The obtained complexes were very slightly soluble in water, methanol, and ethanol and highly soluble in dimethyl sulfoxide (DMSO).

#### 4.2. Analytical and Spectroscopic Methods

The carbon, hydrogen, and nitrogen contents of the obtained complexes were determined by elemental analysis. Solid-state infrared spectra of the studied compounds were recorded in KBr in the 4000–400  $\text{cm}^{-1}$  frequency range by an FTIR IFS25 Bruker spectrometer. Raman spectra of 5-aminoorotic acid and its new La(III) and Ga(III) complexes were recorded with a Dilor microspectrometer (Horiba-Jobin-Yvon, model LabRam) equipped with 1800 grooves/mm holographic grating. The 514.5 nm line of an argon ion laser (Spectra Physics, model 2016) was used for the probes' excitation. The spectra were collected in backscattering geometry with a confocal Raman microscope equipped with an Olympus LMPlanFL 50 $\times$  objective and a resolution of 2  $\text{cm}^{-1}$ . The detection of Raman signal was carried out with a Peltier-cooled CCD camera. Laser power of 100 mW was used in our measurements.  $^1\text{H}$  NMR spectra were recorded at room temperature on a Bruker 250 WM (250 MHz) spectrometer in  $\text{DMSO}-d_6$ . Chemical shifts are given in ppm, downfield from TMS.

#### 4.3. Radical-Scavenging Assays

All materials and compounds were of the finest grade (p.a.) (Sigma-Aldrich). Solutions were prepared in bi-distilled water. The tested concentrations of 5-aminoorotic acid and its complexes with Ga(III) and La(III) were between  $1 \times 10^{-6}$  M and  $1 \times 10^{-4}$  M. The desired concentrations were achieved by dilution of standard aqueous solutions with concentrations  $1 \times 10^{-3}$  M for HAOA and LaAOA and  $3 \times 10^{-4}$  M for GaAOA (the highest concentration possible for GaAOA in water). Then, 25.4 mU/mL xanthine oxidase was dissolved in 50 mM K,Na-phosphate buffer with  $\text{pH} = 7.45$  (PBS) and used in the LDCL and UV-Vis measurements. Directly prior to use, 1 mM  $\text{KO}_2$  solution in dehydrated DMSO was prepared. A 3 mM solution of xanthine was prepared by dissolving the compound in 0.1 N NaOH and further dilution with bi-distilled water. 5-Amino-2,3-dihydro-1,4-phthalazinedione (luminol) was dissolved in a small amount of 0.01 M NaOH, further diluted to  $1 \times 10^{-3}$  M in 50 mM PBS of  $\text{pH} = 7.45$ , and  $\text{pH}$  was adjusted again to 7.45.

LDCL was applied in order to estimate the radical-scavenging activity in the presence of the model systems containing  $\text{KO}_2$  and X/XO. LUMAT LB9507 apparatus was used for the LDCL investigations. The kinetics were measured with delay time 2 s, measuring time 3 s for a total period of 600 s. The integral intensities for the first 10 s were used in data management.

The specific activity of XO in the model system X/XO was estimated by UV spectrophotometric measurements of the relative change in the characteristic signal of uric acid (UA) at 293 nm. This experiment was performed using a UV 1650PC Shimadzu spectrophotometer. The delay time was 10 s, and the activity of the UA formation was computed by the program subroutine for a period of 10–90 s.

##### 4.3.1. Assay for CL in the Presence of $\text{KO}_2$

One milliliter of the control volume contained 0.05 mL  $\text{KO}_2$  solution, 0.05 mL luminol, and PBS. One milliliter of the sample volume contained 0.05 mL  $\text{KO}_2$ , 0.05 mL luminol, the compound investigated in the desirable concentration, and PBS. The results were presented as the chemiluminometric scavenging index (CL-SI), calculated as follows (Equation (3)):

$$\text{CL-SI} = \frac{I_{\text{sample}}}{I_{\text{control}}} \times 100 \quad (3)$$

where  $I_{\text{control}}$  and  $I_{\text{sample}}$  are the integral intensities measured for the  $\text{KO}_2$  alone and in the presence of the compound in a desired concentration. The background measurement showed an integral intensity of 10 and was subtracted from both control and sample measurements.

For each compound at each desirable concentration, 5 parallel measurements were performed. Average values and standard deviations were used for further comparisons.

#### 4.3.2. Assay for CL in the Presence of X/XO Model System

The 1 mL cuvette for the control measurement contained 0.02 mL XO solution, 0.1 mL xanthine, 0.1 mL luminol, and PBS. A 1 mL solution for the sample measurement contained 0.02 mL XO, 0.1 mL X, the compound investigated in the desired concentration, and PBS. The CL-SI was determined using the same formula as shown for the  $\text{KO}_2$  assay. For each desirable concentration of the compounds investigated, 5 parallel measurements were performed. The average values and standard deviations were calculated and used in further comparisons.

#### 4.3.3. Assay for UV Determination of XO Activity in the Presence of the X/XO Model System

One milliliter of the reaction mixture for the control measurement contained 0.02 mL XO, 0.1 mL xanthine, and PBS. The 1 mL cuvette for the sample measurement contained 0.02 mL XO, 0.1 mL X, the compound investigated in a desired concentration, and PBS. As no additional components in this model system were present, only UA and  $\text{O}_2^-$  were produced. As the final product of xanthine transformation was uric acid (UA), the absorption at 293 nm (characteristic wavelength for UA) was measured for 10 min, using the molar extinction coefficient of  $1.22 \times 10^4 \text{ M}^{-1} \cdot \text{cm}^{-1}$  [98]. The activity of XO was defined as the amount of enzyme needed to convert 1  $\mu\text{mole}$  of xanthine for 1 min in a 1 mL reaction mixture at 298 K. Data for the sample activity of XO were presented as a percentage of the XO activity seen in the control measurement.

#### 4.4. Statistical Analysis

Five parallel measurements were performed for each investigated concentration of every substance. Each measurement represented an individual data point. Averages and standard deviations were calculated. Relative changes within the limits of experimental error were ignored. The significance of differences between standard deviations was verified by the Bartlett test. One-way ANOVA, followed by the Bonferoni post-test confirmed the concentration-dependent impact of the substances on the radical-generating model systems. The Bartlett test was used to verify that all standard deviations belonged to the same population. Differences at  $p < 0.05$  were considered as statistically significant.

#### In Silico Molecular Docking Assay

The molecular docking protocol was chosen to be a specific docking type; in this case, full flexibility was given to the inhibitor. The Genetic Optimization Ligand for Docking software (GOLD) [99] protocol involved six steps:

- removing ligands, heteroatoms, and unnecessary water molecules unless needed at the active site (step I);
- checking the receptor ionization and tautomeric states by adding the necessary hydrogen atoms (step II);
- defining the active site by using the list of active site residues mode (step III);
- setting the ligands by performing energy minimization using the Hyperchem v8.0 program [100]. First, we used the single point mode to calculate the ligand energy and gradient, then molecular mechanics optimization was performed using the Polack–Ribiere conjugate gradient algorithm where the RMS gradient of  $0.1 \text{ kcal}/(\text{\AA} \text{ mol})$  was used for 735 cycles (step IV);
- fitness function choice, and the piecewise linear potential (PLPChem score) was chosen as the most recommended fitness function in GOLD [99] (step V);
- the number of genetic algorithm (GA) runs, and 100 solutions (results) per inhibitor were chosen as the most accurate (step VI).

The root mean square deviation (RMSD) and cluster size were kept as the default settings [101]. The best solutions were chosen based on the highest PLPChem score, along with the ratio of the most repeated poses as a percentage. The obtained molecular docking results were analyzed using Discovery Studio Visualizer (DSV), v 4.0 [102].

PLP and ChemPLP are empirical fitness functions, optimized for pose prediction; they model the attraction as well as repulsion of protein and ligand heavy atoms. In both cases, the piecewise linear potential (PLP) is utilized to model the steric complementarity between protein and ligand, while ChemPLP adds the distance- and angle-dependent hydrogen and metal bonding terms. The internal score of the ligand consists of the heavy-atom clash potential (*flig-clash*) [99,103,104] as well as the torsional potential used within ChemScore (*flig-tors*). Both fitness functions are capable of covalent docking (*fchem-cov*), considering flexible side chains (*fchem-prot*) and explicit water molecules as well as handling constraints (*fcons*) [105]. The Discovery Studio Visualizer program was used for result treatments.

**Author Contributions:** Conceptualization, I.K. and K.B.; methodology, I.K., M.T. and K.B.; software, K.B., M.T. and A.L.; validation, L.S., I.K. and K.B.; formal analysis, I.K., L.S. and K.B.; investigation, I.K., M.T., L.T. and A.L.; resources, I.K., M.T., K.B., L.S., A.L. and L.T.; data curation, I.K., M.T. and K.B.; writing—I.K., M.T., K.B. and L.T.; writing—review and editing, L.T.; visualization, I.K., M.T. and K.B.; supervision, I.K. and L.S.; project administration, I.K.; funding acquisition, I.K. All authors have read and agreed to the published version of the manuscript.

**Funding:** This research received no external funding.

**Data Availability Statement:** Not Applicable.

**Conflicts of Interest:** The authors declare no conflict of interest.

**Sample Availability:** Samples of the compounds are not available from the authors.

## References

1. Arouma, O. Free radicals, oxidative stress, and antioxidants in human health and disease. *Nutrition* **2002**, *18*, 872–879. [CrossRef]
2. Valko, M.; Leibfritz, D.; Moncol, J.; Cronin, M.T.; Mazur, M.; Telser, J. Free radicals and antioxidants in normal physiological functions and human disease. *Int. J. Biochem. Cell Biol.* **2007**, *39*, 44–84. [CrossRef] [PubMed]
3. Guzik, T.J.; Korbout, R.; Adamek-Guzik, T. Nitric oxide and superoxide in inflammation and immune regulation. *J. Physiol. Pharmacol.* **2003**, *54*, 469–487.
4. Ullrich, V.; Namgaladze, D.; Frein, D. Superoxide as inhibitor of calcineurin and mediator of redox regulation. *Toxicol. Lett.* **2003**, *139*, 107–110. [CrossRef]
5. Linnane, A.W.; Kios, M.; Vitetta, L. The essential requirement for superoxide radical and nitric oxide formation for normal physiological function and healthy aging. *Mitochondrion* **2007**, *7*, 1–5. [CrossRef]
6. Ullrich, V.; Bachschmid, M. Superoxide as a messenger of endothelial function. *Biochem. Biophys. Res. Commun.* **2000**, *278*, 1–8. [CrossRef] [PubMed]
7. Mayorov, D.N. Brain superoxide as a key regulator of the cardiovascular response to emotional stress in rabbits. *Exp. Physiol.* **2007**, *92*, 471–479. [CrossRef]
8. Brand, M.D. Mitochondrial generation of superoxide and hydrogen peroxide as the source of mitochondrial redox signaling. *Free Radic. Biol. Med.* **2016**, *100*, 14–31. [CrossRef]
9. Porporato, P.E.; Payen, V.L.; Pérez-Escuredo, J.; De Saedeleer, C.J.; Danhier, P.; Copetti, T.; Dhup, S.; Tardy, M.; Vazeille, T.; Bouzin, C.; et al. A mitochondrial switch promotes tumor metastasis. *Cell Rep.* **2014**, *8*, 754–766. [CrossRef]
10. Kosmider, B.; Lin, C.-R.; Karim, L.; Tomar, D.; Vlasenko, L.; Marchetti, N.; Bolla, S.; Madesh, M.; Criner, G.J.; Bahmed, K. Mitochondrial dysfunction in human primary alveolar type II cells in emphysema. *EBioMedicine* **2019**, *46*, 305–316. [CrossRef] [PubMed]
11. Cao, T.; Fan, S.; Zheng, D.; Wang, G.; Yu, Y.; Chen, R.; Song, L.-S.; Fan, G.-C.; Zhang, Z.; Peng, T. Increased calpain-1 in mitochondria induces dilated heart failure in mice: Role of mitochondrial superoxide anion. *Basic Res. Cardiol.* **2019**, *114*, 1–15. [CrossRef]
12. Suski, J.M.; Lebedzinska, M.; Bonora, M.; Pinton, P.; Duszyński, J.; Wieckowski, M.R. Relation between mitochondrial membrane potential and ROS formation. In *Mitochondrial Bioenergetics*; Springer: Berlin/Heidelberg, Germany, 2012; pp. 183–205.
13. Kalyanaraman, B.; Cheng, G.; Hardy, M.; Ouari, O.; Bennett, B.; Zielonka, J. Teaching the basics of reactive oxygen species and their relevance to cancer biology: Mitochondrial reactive oxygen species detection, redox signaling, and targeted therapies. *Redox Biol.* **2018**, *15*, 347–362. [CrossRef] [PubMed]
14. Matés, J.M.; Segura, J.A.; Alonso, F.J.; Márquez, J. Oxidative stress in apoptosis and cancer: An update. *Arch. Toxicol.* **2012**, *86*, 1649–1665. [CrossRef] [PubMed]



15. Indo, H.P.; Yen, H.-C.; Nakanishi, I.; Matsumoto, K.-I.; Tamura, M.; Nagano, Y.; Matsui, H.; Gusev, O.; Cornette, R.; Okuda, T.; et al. A mitochondrial superoxide theory for oxidative stress diseases and aging. *J. Clin. Biochem. Nutr.* **2015**, *56*, 1–7. [[CrossRef](#)]
16. Hayyan, M.; Hashim, M.A.; AlNashef, I.M. Superoxide ion: Generation and chemical implications. *Chem. Rev.* **2016**, *116*, 3029–3085. [[CrossRef](#)]
17. Murrell, G.A.; Francis, M.J.; Bromley, L. Modulation of fibroblast proliferation by oxygen free radicals. *Biochem. J.* **1990**, *265*, 659–665. [[CrossRef](#)]
18. Weening, R.; Wever, R.; Roos, D. Quantitative aspects of the production of superoxide radicals by phagocytizing human granulocytes. *J. Lab. Clin. Med.* **1975**, *85*, 245–252. [[PubMed](#)]
19. Matsubara, T.; Ziff, M. Increased superoxide anion release from human endothelial cells in response to cytokines. *J. Immunol.* **1986**, *137*, 3295–3298.
20. Burdon, R.H. Superoxide and hydrogen peroxide in relation to mammalian cell proliferation. *Free Rad. Biol. Med.* **1995**, *18*, 775–794. [[CrossRef](#)]
21. Day, R.M.; Suzuki, Y.J. Cell proliferation, reactive oxygen and cellular glutathione. *Dose-Response* **2005**, *3*. [[CrossRef](#)]
22. Valko, M.; Rhodes, C.; Moncol, J.; Izakovic, M.; Mazur, M. Free radicals, metals and antioxidants in oxidative stress-induced cancer. *Chem. Biol. Interact.* **2006**, *160*, 1–40. [[CrossRef](#)]
23. Prasad, S.; Gupta, S.C.; Tyagi, A.K. Reactive oxygen species (ROS) and cancer: Role of antioxidative nutraceuticals. *Cancer Lett.* **2017**, *387*, 95–105. [[CrossRef](#)] [[PubMed](#)]
24. Dayem, A.A.; Choi, H.-Y.; Kim, J.-H.; Cho, S.-G. Role of oxidative stress in stem, cancer, and cancer stem cells. *Cancers* **2010**, *2*, 859–884. [[CrossRef](#)]
25. Tafani, M.; Sansone, L.; Limana, F.; Arcangeli, T.; De Santis, E.; Polese, M.; Fini, M.; Russo, M.A. The interplay of reactive oxygen species, hypoxia, inflammation, and sirtuins in cancer initiation and progression. *Oxid. Med. Cell. Longev.* **2016**, *2016*, 1–18. [[CrossRef](#)] [[PubMed](#)]
26. Nazarewicz, R.R.; Dikalova, A.; Bikineyeva, A.; Ivanov, S.; Kirilyuk, I.A.; Grigor'ev, I.A.; Dikalov, S.I. *Does Scavenging of Mitochondrial Superoxide Attenuate Cancer Prosurvival Signaling Pathways?*; Mary Ann Liebert, Inc.: New Rochelle, NY, USA, 2013.
27. Shah, M.H.; Liu, G.-S.; Thompson, E.W.; Dusting, G.J.; Peshavariya, H.M. Differential effects of superoxide dismutase and superoxide dismutase/catalase mimetics on human breast cancer cells. *Breast Cancer Res. Treat.* **2015**, *150*, 523–534. [[CrossRef](#)] [[PubMed](#)]
28. Gill, J.G.; Piskounova, E.; Morrison, S.J. (Eds.) *Cancer, Oxidative Stress, and Metastasis. Cold Spring Harbor Symposia on Quantitative Biology*; Cold Spring Harbor Laboratory Press: Cold Spring Harbor, NY, USA, 2016.
29. Sosa, V.; Moliné, T.; Somoza, R.; Paciucci, R.; Kondoh, H.; LLeonart, M.E. Oxidative stress and cancer: An overview. *Ageing Res. Rev.* **2013**, *12*, 376–390. [[CrossRef](#)] [[PubMed](#)]
30. Luis, A.; Sandalio, L.M.; Palma, J.; Bueno, P.; Corpas, F.J. Metabolism of oxygen radicals in peroxisomes and cellular implications. *Free Radic. Biol. Med.* **1992**, *13*, 557–580.
31. Kostić, D.A.; Dimitrijević, D.S.; Stojanović, G.S.; Palić, I.R.; Đorđević, A.S.; Ickovski, J.D. Xanthine oxidase: Isolation, assays of activity, and inhibition. *J. Chem.* **2015**, *2015*. [[CrossRef](#)]
32. Cos, P.; Ying, L.; Calomme, M.; Hu, J.P.; Cimanga, K.; Van Poel, B.; Pieters, L.; Vlietinck, A.J.; Berghe, D.V. Structure–activity relationship and classification of flavonoids as inhibitors of xanthine oxidase and superoxide scavengers. *J. Nat. Prod.* **1998**, *61*, 71–76. [[CrossRef](#)]
33. Mittal, A.; Phillips, A.R.; Loveday, B.; Windsor, J.A. The potential role for xanthine oxidase inhibition in major intra-abdominal surgery. *World J. Surg.* **2008**, *32*, 288–295. [[CrossRef](#)]
34. Candan, F. Effect of *Rhus coriaria* L.(Anacardiaceae) on superoxide radical scavenging and xanthine oxidase activity. *J. Enzyme Inhib. Med. Chem.* **2003**, *18*, 59–62. [[CrossRef](#)]
35. Kelley, E.E.; Khoo, N.K.; Hundley, N.J.; Malik, U.Z.; Freeman, B.A.; Tarpey, M.M. Hydrogen peroxide is the major oxidant product of xanthine oxidase. *Free Rad. Biol. Med.* **2010**, *48*, 493–498. [[CrossRef](#)]
36. Xu, H.; Li, C.; Mozziconacci, O.; Zhu, R.; Xu, Y.; Tang, Y.; Chen, R.; Huang, Y.; Holzbeierlein, J.M.; Schöneich, C.; et al. Xanthine oxidase-mediated oxidative stress promotes cancer cell-specific apoptosis. *Free Rad. Biol. Med.* **2019**, *139*, 70–79. [[CrossRef](#)]
37. Oh, S.-H.; Choi, S.-Y.; Choi, H.-J.; Ryu, H.-M.; Kim, Y.-J.; Jung, H.-Y.; Cho, J.-H.; Kim, C.-D.; Park, S.-H.; Kwon, T.-H.; et al. The emerging role of xanthine oxidase inhibition for suppression of breast cancer cell migration and metastasis associated with hypercholesterolemia. *FASEB J.* **2019**, *33*, 7301–7314. [[CrossRef](#)]
38. Ogura, J.; Kuwayama, K.; Sasaki, S.; Kaneko, C.; Koizumi, T.; Yabe, K.; Tsujimoto, T.; Takeno, R.; Takaya, A.; Kobayashi, M.; et al. Reactive oxygen species derived from xanthine oxidase interrupt dimerization of breast cancer resistance protein, resulting in suppression of uric acid excretion to the intestinal lumen. *Biochem. Pharmacol.* **2015**, *97*, 89–98. [[CrossRef](#)] [[PubMed](#)]
39. Furue, H. Chemotherapy cancer treatment during the past sixty years. *Cancer Chemother.* **2003**, *30*, 1404–1411.
40. Wiemann, M.; Calabresi, P. Principles of current cancer chemotherapy. *Compr. Ther.* **1983**, *9*, 46–52. [[PubMed](#)]
41. Tanneberger, S. Cancer chemotherapy today and in the future. *Z. Gesamte Inn. Med. Grenzgeb.* **1990**, *45*, 693–695.
42. Kim, S.J.; Kim, H.S.; Seo, Y.R. Understanding of ROS-inducing strategy in anticancer therapy. *Oxid. Med. Cell. Longev.* **2019**, *2019*, 5381692. [[CrossRef](#)]
43. Wang, K.; Li, R.; Cheng, Y.; Zhu, B. Lanthanides—The future drugs? *Coord. Chem. Rev.* **1999**, *190*, 297–308. [[CrossRef](#)]
44. Kostova, I. Lanthanides as anticancer agents. *Curr. Med. Chem.* **2005**, *5*, 591–602. [[CrossRef](#)]

45. Todorov, L.; Kostova, I.; Traykova, M. Lanthanum, Gallium and their Impact on Oxidative Stress. *Curr. Med. Chem.* **2019**, *26*, 4280–4295. [[CrossRef](#)]
46. Lessa, J.A.; Parrilha, G.L.; Beraldo, H. Gallium complexes as new promising metallodrug candidates. *Inorg. Chim. Acta* **2012**, *393*, 53–63. [[CrossRef](#)]
47. Kapoor, S. Lanthanum and its rapidly emerging role as an anti-carcinogenic agent. *J. Cell. Biochem.* **2009**, *106*, 193. [[CrossRef](#)] [[PubMed](#)]
48. Durgo, K.; Halec, I.; Šola, I.; Franekić, J. Cytotoxic and genotoxic effects of the quercetin/lanthanum complex on human cervical carcinoma cells in vitro. *Arhiv za Higijenu Rada i Toksikologiju* **2011**, *62*, 221–226. [[CrossRef](#)]
49. Shen, L.; Lan, Z.; Sun, X.; Shi, L.; Liu, Q.; Ni, J. Proteomic analysis of lanthanum citrate-induced apoptosis in human cervical carcinoma SiHa cells. *Biomaterials* **2010**, *23*, 1179–1189. [[CrossRef](#)]
50. Valcheva-Traykova, M.; Saso, L.; Kostova, I. Involvement of lanthanides in the free radicals' homeostasis. *Curr. Top. Med. Chem.* **2014**, *14*, 2508–2519. [[CrossRef](#)] [[PubMed](#)]
51. Todorov, L.; Chifchiev, B.; Valcheva-Traykova, M.; Kostova, I. Radical scavenging activity toward 2, 2-diphenyl-1-picrylhydrazyl and hydroxyl radicals of 5 aminoorotic acid and its Ga (III) complex. *Bulg. Chem. Commun.* **2018**, *50*, 207–212.
52. Todorov, L.; Valcheva-Traykova, M.; Traykov, T.; Kostova, I. Impact of 5-aminoorotic acid and its complex with gallium (III) on the luminol-dependent chemiluminescence in presence of sodium hypochlorite. *AIP Conf. Proc.* **2019**, *2075*, 170004.
53. Todorov, L.; Valcheva-Traykova, M.; Atanasova, V.; Kostova, I. Effect of 5-aminoorotic acid and its gallium (III) complex on the antioxidant activity of rat blood serum. *Bulg. Chem. Commun.* **2019**, *51*, 200–203.
54. Todorov, L.; Valcheva-Traykova, M.; Kostova, I. In Vitro Interaction of 5-aminoorotic Acid and Its Lanthanum(III) Complex With Superoxide and Hypochlorite Radicals. *Pharma Chem.* **2020**, *12*, 10.
55. Todorov, L.; Traykova, M.; Saso, L.; Kostova, I. In Vitro Interaction of 5-Aminoorotic Acid and Its Gallium (III) Complex with Superoxide Radical, Generated by Two Model Systems. *Int. J. Mol. Sci.* **2020**, *21*, 8862. [[CrossRef](#)]
56. Hernanz, A.; Billes, F.; Bratu, I.; Navarro, R. Vibrational analysis and spectra of orotic acid. *Biopolymers* **2000**, *57*, 187–198. [[CrossRef](#)]
57. Takusagawa, F.; Shimada, A. The crystal structure of orotic acid monohydrate (Vitamin B13). *Bull. Chem. Soc. Jpn.* **1973**, *46*, 2011–2019. [[CrossRef](#)]
58. Hilal, R.; Zaky, Z.; Elroby, S.A. Electronic structure of orotic acid I. Geometry, conformational preference and tautomerism. *J. Mol. Struct. THEOCHEM* **2004**, *685*, 35–42.
59. Dinda, J.; Bag, K.; Sinha, C.; Mostafa, G.; Lu, T.-H. Naphthylazoimidazole and mercury (II) complexes. Single crystal X-ray structure of 1-ethyl-2-(naphthyl- $\alpha$ -azo) imidazolium hexafluorophosphate. *Polyhedron* **2003**, *22*, 1367–1376. [[CrossRef](#)]
60. Wysokiński, R.; Morzyk-Ociepa, B.; Głowiak, T.; Michalska, D. Revised molecular structure and vibrational spectra of tetraaqua (orotato) nickel (II) monohydrate: Band assignment based on density functional calculations. *J. Mol. Struct.* **2002**, *606*, 241–251. [[CrossRef](#)]
61. Allen, F.H.; Kennard, O.; Watson, D.G.; Brammer, L.; Orpen, A.G.; Taylor, R. Tables of bond lengths determined by X-ray and neutron diffraction. Part 1. Bond lengths in organic compounds. *J. Chem. Soc. Perkin Trans. 2* **1987**, S1–S19. [[CrossRef](#)]
62. Baran, E.J.; Mercader, R.C.; Hueso-Uren, F.; Moreno-Carretero, M.N.; Quiros-Olozabal, M.; Salas-Peregrin, J.M. Crystal structure, raman and  $^{57}\text{Fe}$  Mössbauer spectra of the Fe(II) complex of iso-orotic acid. *Polyhedron* **1996**, *15*, 1717–1721. [[CrossRef](#)]
63. Schneider, A.G.; Schmalke, H.W.; Arod, F.; Dubler, E. The interaction of 5-fluoroorotic acid with transition metals: Synthesis and characterisation of Ni (II), Cu (II) and Zn (II) complexes. *J. Inorg. Biochem.* **2002**, *89*, 227–236. [[CrossRef](#)]
64. Allen, F.H.; Kirby, A.J. Bond length and reactivity. Variable length of the carbon-oxygen single bond. *J. Am. Chem. Soc.* **1984**, *106*, 6197–6200. [[CrossRef](#)]
65. Suter, H.U.; Nonella, M. A Quantum Chemical Investigation of the C–O Bond Length and Stretching Mode of the Phenolate Anion. *J. Phys. Chem. A* **1998**, *102*, 10128–10133. [[CrossRef](#)]
66. Djordjevic, C.; Vuletic, N.; Jacobs, B.A.; Lee-Renslo, M.; Sinn, E. Molybdenum (VI) peroxo  $\alpha$ -amino acid complexes: Synthesis, spectra, and properties of  $\text{MoO}(\text{O}_2)_2$  ( $\alpha$ -aa) ( $\text{H}_2\text{O}$ ) for  $\alpha$ -aa = glycine, alanine, proline, valine, leucine, serine, asparagine, glutamine, and glutamic acid. X-ray crystal structures of the glycine, alanine, and proline compounds. *Inorg. Chem.* **1997**, *36*, 1798–1805.
67. Kieninger, M.; Ventura, O.N.; Suhai, S. Density functional investigations of carboxyl free radicals: Formyloxyl, acetyloxyl, and benzoyloxyl radicals. *Int. J. Quantum Chem.* **1998**, *70*, 253–267. [[CrossRef](#)]
68. Darensbourg, D.J.; Draper, J.D.; Larkins, D.L.; Frost, B.J.; Reibenspies, J.H. Organometallic Derivatives of Orotic Acid. CO–Labilizing Ability of the Amido Group in Chromium and Tungsten Carbonyl Complexes. *Inorg. Chem.* **1998**, *37*, 2538–2546. [[CrossRef](#)]
69. Bekiroglu, S.; Kristiansson, O. Hydrogen-bonded neutral and anionic lamellar networks: Crystal structures of bis (O, O', O''-hydroorotato) disilver (i) dihydrate, potassium hydroorotate and rubidium hydroorotate. Ab initio calculations on orotic acid and the hydroorotate anion. *J. Chem. Soc. Dalton Trans.* **2002**, 1330–1335. [[CrossRef](#)]
70. Arrizabalaga, P.; Castan, P.; Dahan, F. Coordination sites of 5-nitro-6-carboxyuracil: UV study and x-ray structure determination of diammine (5-nitroorotato) copper (II) hydrate and hexaamminebis (5-nitroorotato) tricopper (II) pentahydrate. *Inorg. Chem.* **1983**, *22*, 2245–2252. [[CrossRef](#)]

71. Lewandowski, W.; Kalinowska, M.; Lewandowska, H. The influence of metals on the electronic system of biologically important ligands. Spectroscopic study of benzoates, salicylates, nicotines and isoorotates. Review. *J. Inorg. Biochem.* **2005**, *99*, 1407–1423. [[CrossRef](#)]
72. Lalioti, N.; Raptopoulou, C.P.; Terzis, A.; Panagiotopoulos, A.; Perlepes, S.P.; Manessi-Zoupa, E. New metal-binding modes for 5-aminoorotic acid: Preparation, characterization and crystal structures of zinc (II) complexes. *J. Chem. Soc. Dalton Trans.* **1998**, 1327–1334. [[CrossRef](#)]
73. Dega-Szafran, Z.; Dulewicz, E.; Dutkiewicz, G.; Kosturkiewicz, Z.; Szafran, M. Two polymorphs of 4-hydroxy-1-methylpiperidine betaine hydrochloride studied by X-ray and DFT methods. *J. Mol. Struct.* **2005**, *751*, 139–150. [[CrossRef](#)]
74. Horn, K.H.; Böres, N.; Lehnert, N.; Mersmann, K.; Näther, C.; Peters, G.; Tuczek, F. Reduction Pathway of End-On Terminally Coordinated Dinitrogen. IV. Geometric, Electronic, and Vibrational Structure of a W (IV) Dialkylhydrazido Complex and Its Two-Electron-Reduced Derivative Undergoing N–N Cleavage upon Protonation. *Inorg. Chem.* **2005**, *44*, 3016–3030. [[CrossRef](#)]
75. Batt, R.D.; Martin, J.K.; Ploeser, J.M.; Murray, J. Chemistry of the Dihydropyrimidines. Ultraviolet Spectra and Alkaline Decomposition 1a. *J. Am. Chem. Soc.* **1954**, *76*, 3663–3665. [[CrossRef](#)]
76. Icbudak, H.; Olmez, H.; Yesilel, O.Z.; Arslan, F.; Naumov, P.; Jovanovski, G.; Ibrahim, A.R.; Usman, A.; Fun, H.K.; Chantrapromma, S.; et al. Syntheses, characterization and crystal structures of novel amine adducts of metal saccharinates, orotates and salicylates. *J. Mol. Struct.* **2003**, *657*, 255–270. [[CrossRef](#)]
77. Papaefstathiou, G.S.; Manessi, S.; Raptopoulou, C.P.; Behrman, E.J.; Zafiroopoulos, T.F. The first metal complex of 5-hydroxyorotic acid: Dimethylammonium bis (N, N-dimethylformamide) bis (5-hydroxyorotato (-2)) gallate (III). *Inorg. Chem. Commun.* **2004**, *7*, 69–72. [[CrossRef](#)]
78. Lacher, J.; Bitner, J.; Park, J. The Infrared Absorption Spectra of Some Antibiotics in Antimony Trichloride Solution. *J. Phys. Chem.* **1955**, *59*, 610–614. [[CrossRef](#)]
79. Lencioni, S.; Pellerito, A.; Fiore, T.; Giuliani, A.; Pellerito, L.; Cambria, M.T.; Mansueto, C. Organometallic complexes with biological molecules. X: Dialkyltin (IV) and trialkyltin (IV) orotates: Spectroscopic and in vivo investigations. *Appl. Organomet. Chem.* **1999**, *13*, 145–157. [[CrossRef](#)]
80. Kostova, I.; Peica, N.; Kiefer, W. Theoretical and spectroscopic studies of lanthanum (III) complex of 5-aminoorotic acid. *Chem. Phys.* **2006**, *327*, 494–505. [[CrossRef](#)]
81. Lewandowski, W.; Barańska, H. Comparison of the influence of silver, iron (III) and chromium (III) on the aromatic system of benzoic and salicylic acids in hydrated and anhydrous complexes. *Vib. Spectrosc.* **1991**, *2*, 211–220. [[CrossRef](#)]
82. Lewandowski, W.; Dasiewicz, B.; Koczoń, P.; Skierski, J.; Dobrosz-Teperek, K.; Świsłocka, R.; Fuks, L.; Priebe, W.; Mazurek, A. Vibrational study of alkaline metal nicotines, benzoates and salicylates. *J. Mol. Struct.* **2002**, *604*, 189–193. [[CrossRef](#)]
83. Koczon, P.; Lewandowski, W.; Mazurek, A. Vibrational (FT-IR and FT-Raman) and NMR studies on selected metal (Ca, Mn, Zn) complexes with ortho-, meta-, and para-iodobenzoic acids. *Vib. Spectrosc.* **1999**, *20*, 143–149. [[CrossRef](#)]
84. Kakiuchi, M.; Abe, T.; Nakayama, H. D/H fractionation factor between water vapor and crystal water of copper chloride dihydrate: Statistical mechanical approach based on Raman spectra. *Geochem. J.* **2001**, *35*, 285–293. [[CrossRef](#)]
85. Wang, K.; Li, Y.-S. Silver doping of polycarbonate films for surface-enhanced Raman scattering. *Vib. Spectrosc.* **1997**, *14*, 183–188. [[CrossRef](#)]
86. Boerio, F.; Hong, P.; Clark, P.; Okamoto, Y. Surface-enhanced Raman scattering from model acrylic adhesive systems. *Langmuir* **1990**, *6*, 721–727. [[CrossRef](#)]
87. Kwon, Y.J.; Son, D.H.; Ahn, S.J.; Kim, M.S.; Kim, K. Vibrational spectroscopic investigation of benzoic acid adsorbed on silver. *J. Phys. Chem.* **1994**, *98*, 8481–8487. [[CrossRef](#)]
88. Gałdecka, E.; Gałdecki, Z.; Huskowska, E.; Amirhanov, V.; Legendziejewicz, J. Crystal structure and optical properties of Ln (III) octahedral complexes with hexamethylphosphorotriamide; [Ln (HMPA)<sub>6</sub>](ClO<sub>4</sub>)<sub>3</sub>. *J. Alloys Compd.* **1997**, *257*, 182–190. [[CrossRef](#)]
89. De Andres, A.; Taboada, S.; Martínez, J.; Salinas, A.; Hernández, J.; Sáez-Puche, R. Optical phonons in R<sub>2</sub>BaMO<sub>5</sub> oxides with M = Co, Ni, Cu, and R = a rare earth. *Phys. Rev. B* **1993**, *47*, 14898. [[CrossRef](#)]
90. Cho, B.-O.; Lao, S.X.; Chang, J.P. Origin and effect of impurity incorporation in plasma-enhanced ZrO<sub>2</sub> deposition. *J. Appl. Phys.* **2003**, *93*, 9345–9351. [[CrossRef](#)]
91. Barfield, M. *Proton and Carbon-13 nmr Spectroscopy*; Abraham, R.J., Loftus, P., Eds.; ACS Publications: Washington, DC, USA, 1979.
92. Jackman, L.M.; Sternhell, S. *Application of Nuclear Magnetic Resonance Spectroscopy in Organic Chemistry: International Series in Organic Chemistry*; Elsevier: Amsterdam, The Netherlands, 2013.
93. Enroth, C.; Eger, B.T.; Okamoto, K.; Nishino, T.; Nishino, T.; Pai, E.F. Crystal structures of bovine milk xanthine dehydrogenase and xanthine oxidase: Structure-based mechanism of conversion. *Proc. Natl. Acad. Sci. USA* **2000**, *97*, 10723–10728. [[CrossRef](#)] [[PubMed](#)]
94. Linani, A.; Benarous, K.; Bou-Salah, L.; Yousfi, M. Hispidin, Harmaline, and Harmine as potent inhibitors of bovine xanthine oxidase: Gout treatment, in vitro, ADMET prediction, and SAR studies. *Bioorg. Chem.* **2021**, *112*, 104937. [[CrossRef](#)] [[PubMed](#)]
95. Bou-Salah, L.; Benarous, K.; Linani, A.; Rabhi, F.; Chaib, K.; Chine, I.; Bensaidane, H.; Yousfi, M. Anti-inflammatory drugs as new inhibitors to xanthine oxidase: In vitro and in silico approach. *Mol. Cell. Probes* **2021**, *58*, 101733. [[CrossRef](#)]
96. Bou-Salah, L.; Benarous, K.; Linani, A.; Bombarda, I.; Yousfi, M. In vitro and in silico inhibition studies of five essential oils on both enzymes human and bovine xanthine oxidase. *Ind. Crops Prod.* **2020**, *143*, 111949. [[CrossRef](#)]

97. Benarous, K.; Bou-Salah, L.; Linani, A.; Yousfi, M.; Kostova, I.; Saso, L. Lanthanide (III) complexes of bis-coumarins as strong inhibitors of bovine xanthine oxidase-molecular docking and SAR studies. *J. Biomol. Struct. Dyn.* **2020**, 1–7. [[CrossRef](#)] [[PubMed](#)]
98. Shintani, H. Determination of xanthine oxidase. *Pharm. Anal. Acta* **2013**, 7, 4. [[CrossRef](#)]
99. Jones, G.; Willett, P.; Glen, R.C.; Leach, A.R.; Taylor, R. Development and validation of a genetic algorithm for flexible docking. *J. Mol. Biol.* **1997**, 267, 727–748. [[CrossRef](#)]
100. *HyperChem(TM) Professional 8.0*; Hypercube, Inc.: Gainesville, FL, USA, 2002.
101. Khedidja, B.; Abderrahman, L. Selection of orlistat as a potential inhibitor for lipase from *Candida* species. *Bioinformation* **2011**, 7, 125. [[CrossRef](#)] [[PubMed](#)]
102. Dassault Systèmes BIOVIA, *BIOVIA Workbook, Release 2017*; BIOVIA Pipeline Pilot—Dassault Systèmes: San Diego, CA, USA, 2017.
103. Korb, O.; Stutzle, T.; Exner, T.E. Empirical scoring functions for advanced protein–ligand docking with PLANTS. *J. Chem. Inf. Model.* **2009**, 49, 84–96. [[CrossRef](#)] [[PubMed](#)]
104. Jones, G.; Willett, P.; Glen, R.C. Molecular recognition of receptor sites using a genetic algorithm with a description of desolvation. *J. Mol. Biol.* **1995**, 245, 43–53. [[CrossRef](#)]
105. Verdonk, M.L.; Cole, J.C.; Hartshorn, M.J.; Murray, C.W.; Taylor, R.D. Improved protein–ligand docking using GOLD. *Proteins* **2003**, 52, 609–623. [[CrossRef](#)]